Eur. Phys. J. B **6**, 341–345 (1998)

**THE EUROPEAN PHYSICAL JOURNAL B**
© EDP Sciences
Springer-Verlag 1998

# Helically modulated electroclinical effects in twist grain boundary liquid crystals

M. Petit[1], M. Nobili[2], and P. Barois[1]

[1] Centre de Recherche Paul Pascal - CNRS, avenue A. Schweitzer, 33600 Pessac, France
[2] Institut Non-Linéaire de Nice, Sophia-Antipolis, 1361 route des Lucioles, 06560 Valbonne, France

Received: 24 April 1998 / Revised: 22 June 1998 / Accepted: 31 July 1998

**Abstract.** We report the first observation of an electroclinical effect at the $TGB_C$–$TGB_A$ transition induced by an external DC electric field applied perpendicular to the pitch direction. Upon increasing the field, the smectic layers rather than the director field tilt over relative to the helical axis, allowing to detect the effect by X-ray scattering from well aligned samples. The observations are qualitatively interpreted in the frame of a mean field phenomenological model of a helically modulated electroclinical effect.

**PACS.** 61.30.Gd Orientational order of liquid crystals; electric and magnetic field effects on order – 64.70.Md Transitions in liquid crystals

In 1977 Garoff and Meyer [1] demonstrated the existence of an electroclinic effect above the smectic A–smectic C* (SmA–SmC*) transition in a chiral liquid crystal. The electroclinical effect is a continuous rotation of the smectic optical axis in response to an electric field applied parallel to the layer planes. The electric field couples linearly to the local dipole moment by inducing a nonzero director tilt proportional to the electric field amplitude. The electroclinical phenomenon has been extensively investigated in the bulk [2–4] and at surfaces [5–8] of SmA and other layered phases; it has even been observed in cholesteric phases [9–13] but not yet reported in Twist Grain Boundary smectic phases (TGB) for which electric field induced transition to the unwound ferroelectric SmC* state has instead been described [14].

The TGB state represents the liquid crystal analog to the Abrikosov flux phase appearing in type II superconductors [15]. The TGB phase is made of smectic slabs (*i.e.* superconducting phase in the analogy) regularly stacked in a helical fashion along an axis $x$ perpendicular to the slab boundaries. Adjacent slabs are continuously connected *via* a grain boundary constituted of a grid of parallel equispaced screw dislocation lines analogous to magnetic vortices. Two TGB phases have been predicted [15] and experimentally identified: the $TGB_A$ [16] and $TGB_C$ phases [17]. The $TGB_A$ is characterized by SmA slabs. The nematic director $\mathbf{n}$ is parallel to the normal to the smectic planes $\mathbf{N}$ and both are perpendicular to the pitch direction $x$. In the $TGB_C$ phase, instead, the slabs have a SmC structure with a SmC tilt angle $\theta$ defined by $\cos\theta = \mathbf{n}\cdot\mathbf{N}$. The smectic layers are tilted by an angle $\omega_L$ with respect to $x$ [18]. The $TGB_C$ structure has *a priori* one more degree of freedom than $TGB_A$ namely the orientation of the vector $\mathbf{n}\times\mathbf{N}$ parallel to the spontaneous electric polarization $\mathbf{P}_S$ of each slab. It was suggested in reference [18] that $\mathbf{n}$ in the $TGB_C$ phase remains orthogonal to the helical axis $x$ like in the $TGB_A$ and cholesteric phases. This assumption which minimizes the bend term of the Frank energy is possible since $\omega_L$ equals $\theta$ within experimental accuracy. As a consequence, the spontaneous electric polarization $\mathbf{P}_S$ of each SmC slab is orthogonal to the pitch axis and precesses in a helical fashion about it (see Fig. 1). Interestingly, such *helielectric* structure can be checked by applying an external transverse electric field $\mathbf{E}$ which couples to the spontaneous polarizations of each smectic slab [19,20]. The electric energy term per unit surface of the $i$th slab reads:

$$\int_{\substack{slab\ i\\ thickness}} -\mathbf{P}_{Si}\cdot\mathbf{E}\,dx = -P_{Si}Es_i\cos\chi_i \qquad (1)$$

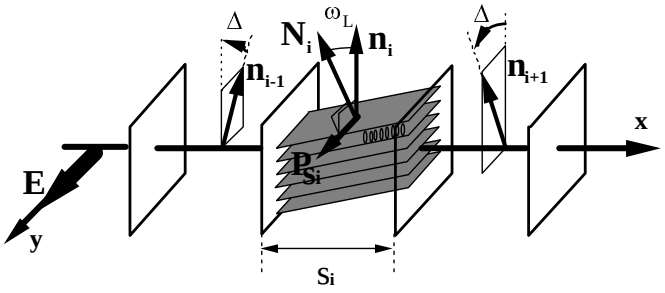


**Fig. 1.** Helielectric model of the $TGB_C$ phase: local spontaneous polarizations $\mathbf{P}_{Si}$ are perpendicular to the pitch axis $x$ at an angle $\chi_i$ relative to the electric field $\mathbf{E}$ (along $y$). $\omega_L$ is the angle of the smectic layer with respect to $x$.

where $s_i$ is the $i$th slab thickness, and $\chi_i$ is the angle between the spontaneous polarization $\mathbf{P}_{Si}$ and the electric field direction, chosen along $y$. In order to minimize the electric energy (1) three different mechanisms are possible: (i) a modulation of the thickness $s_i$ of the slabs: according to the sign of their electric energy, slabs with positive (negative) $\cos\chi_i$ will expand (shrink) (ii) a rotation of the slabs about the screw axis $x$ under the effect of the electric torque in order to increase $\cos\chi_i$ and (iii) a modulation $\delta P_{Si}$ of the modulus $P_{Si}$ of the local polarization, according again to the sign of the electric energy (*i.e.* the product $\delta P_{Si}\cos\chi_i$ must be positive). The first two effects have been observed and characterized in $TGB_C$ phases [19,20]. The third effect corresponds to an electroclinical distortion as will be discussed in the following.

In the $TGB_C$ phase, the electric polarization modulus $P_{Si}$ is proportional to $|\mathbf{n}_i \times \mathbf{N}_i| = \sin\theta_i$. An external electric field parallel to $\mathbf{P}_{Si}$ will increase the local polarization $P_{Si}$ of slab number $i$ *via* a corresponding variation of the tilt $\theta_i$. This is the well known electroclinical effect. Its magnitude is proportional to the component $E\cos\chi_i$ of the field along $\mathbf{P}_{Si}$. It is thus expected to be modulated with $\chi_i$. A similar behavior occurs for the $TGB_A$ phase. The $TGB_A$ has no spontaneous polarization since $|\mathbf{n}_i \times \mathbf{N}_i| = 0$. Nevertheless a polarization $\delta P_{Si}$ and the corresponding tilt can be induced by an external electric field. Both should likewise be modulated by the helical structure of the $TGB_A$. In analogy with the electroclinic effect of a chiral SmA, we call this phenomenon *helically modulated electroclinic effect*. The local SmC tilt $\theta_i$ can *a priori* be changed by reorienting $\mathbf{n}_i$, $\mathbf{N}_i$ or both. A rotation of the director $\mathbf{n}_i$ out of the $y$-$z$ plane costs a large elastic energy of bend. On the other hand, a $\mathbf{N}_i$-reorientation costs only a little increase in the grain boundary energy. The latter mechanism is therefore expected to prevail, allowing X-ray diffraction an easy detection (unlike usual electroclinical effect in non twisted chiral smectics).

In this letter we report an experimental study of the helically modulated electroclinic effect in a TGB phase. The experimental results are qualitatively explained by a simple phenomenogical model.

The electroclinical effect is known to be maximum close to a SmA–SmC* transition where the tilt susceptibility is large. We therefore chose a compound with a continuous $TGB_A$–$TGB_C$ transition. The experiment was performed with the $R$-eniantiomer of the $n = 11$ homolog of the series studied by the Bordeaux group [17,18], 3-fluoro-4-[($R$) or ($S$)-1-methylheptyloxy]-4′-(4″-alkoxy-2″, 3″-difluorobenzoyloxy) tolan (nF2BTFO1M7 for short). The phase sequence on cooling is: isotropic (112.4 °C) blue phases (105.7 °C) N* (104 °C) $TGB_A$ (101.5 °C) $TGB_C$ (100.1 °C) $S_C$* (46.4 °C) crystal. Well aligned samples were prepared as discussed elsewhere [21] between thin (50 $\mu$m) flat pieces of polymer coated and unidirectionally buffed glass. The thickness of the liquid crystal film was fixed by two calibrated spacers: we used 25 $\mu$m parallel gold wires, 3 mm apart and parallel to the direction of rubbing. The quality of the alignment, with helical axis $x$ perpendicular to the cell walls was checked optically under polarizing microscope. The wires were connected to a DC power supply in order to produce an electric field along a direction perpendicular to $x$. The cells were then introduced in a two stage oven (±10 mK accuracy) mounted on the X-ray spectrometer. Experiments were performed using Cu-K$\alpha$ radiation of an 18 kW rotating anode X-ray generator. The samples were mounted on a 4-circle goniometer. The scattered intensity was analyzed by vertical slits and collected by a scintillator. The scattering vector $\mathbf{Q}$ is defined by the axes $Q_x$, $Q_y$ and $Q_z$ (see inset of Fig. 2b for the $TGB_C$ structure). $\omega$ and $\chi$ are the rocking angles about the vertical ($Q_y$) and horizontal ($Q_x$)

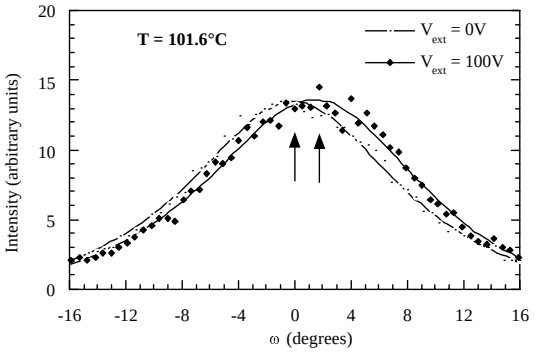


(a)

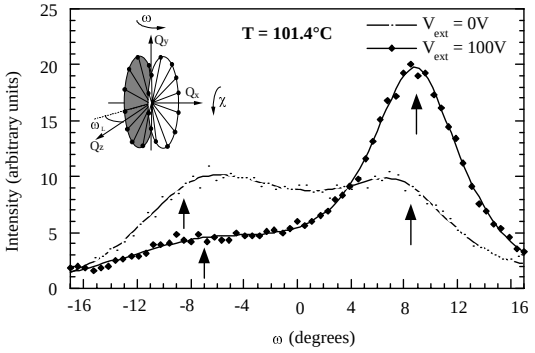


(b)

**Fig. 2.** Rocking curves ($\omega$-scans) recorded at constant wavevector transfer $Q_S = 0.164$ Å$^{-1}$ across the ring of scattering in the plane ($Q_x$, $Q_z$) perpendicular to the field direction ($\chi = 0$) for external voltage $V_{ext} = 0$ V and $V_{ext} = 100$ V. (a) $T = 101.6\,^\circ$C in the $TGB_A$ phase: at zero field (dots), the scattering profile is well fitted to a Gaussian lineshape (solid line) centered at $\omega = 0$. In the field (filled diamonds), the Gaussian profile is preserved, but shifted by 1.8 degrees, well beyond the uncertainty on the position of the maximum (of order 0.3 degrees). (b) $T = 101.4\,^\circ$C in the $TGB_C$ phase: at zero field (dots), the profile exhibits two maxima centered at $\omega_L \approx \pm 8.5$ degrees. It is reasonably well fitted to two overlapping Lorentzian functions (solid line). In the field (filled diamonds), the two maxima are shifted both in intensity and angular position ($\omega$). The variation of the intensity are due to field induced translations of the grain boundaries [19]. Arrows indicate the center of the Gaussian or Lorentzian fitting function. Inset shows scattering geometry and reciprocal lattice of the $TGB_C$ structure.

axes respectively. The X-ray optics of the spectrometer was optimized to probe the angular distribution of the layer normal ($\omega$-scans) at constant momentum transfer: the size of the X-ray beam at sample position was set to $1 \times 2$ mm$^2$. The in-plane resolution was then broad enough ($1.0 \times 10^{-2}$ Å$^{-1}$ FWHM) to avoid two-theta (*i.e.* counter position) corrections with electric field or temperature. Samples are mounted with the rubbing direction parallel to the $z$-axis.

We first performed a series of $\omega$-scans with no applied voltage ($V_{ext} = 0$) [22]. The liquid crystal sample was cooled down slowly by steps of 0.1 °C from the N$^*$ phase into the $TGB_A$ phase, then into the $TGB_C$ phase. In the $TGB_A$ phase, the intensity profiles show a broad peak centered at $\omega = 0$ (circles in Fig. 2a). Upon cooling down to the $TGB_C$ phase, the signal splits up into two broad symmetrical peaks close to the $TGB_A$–$TGB_C$ transition which occurs at temperature $T_{AC}$ (circles in Fig. 2b). Deeper in the $TGB_C$ phase, finally, the two symmetrical peaks get sharper at positions $\pm\omega_L$. $\omega_L$ represents the tilt angle of the smectic layers relative to the pitch axis. In the $TGB_C$ phase, the two maxima $\pm\omega_L$ correspond to slabs with scattering vector $\mathbf{Q}$ at angles $(+\omega_L, \chi)$ and $(-\omega_L, \chi)$, the latter orientation being equivalent to $(+\omega_L, \chi + \pi)$ due to the symmetry $\mathbf{Q} \leftrightarrow -\mathbf{Q}$. $\omega_L$ can be taken as the order parameter of the $TGB_A$–$TGB_C$ transition.

We then applied a DC voltage $V_{ext}$ across the gold electrodes to induce a positive electric field along the $y$-axis. The origin of the $\chi$ circle is chosen for vertical external field. For each voltage value, a series of $\omega$-scans at $\chi = 0$ was recorded by increasing the temperature by steps of 0.1 °C from 100.9 °C in the middle of the $TGB_C$ phase to 102.2 °C in the $TGB_A$ phase. Two $\omega$-scans recorded for $V_{ext} = 100$ V are shown in Figure 2 (filled diamonds). Temperature values are the same as for $V_{ext} = 0$ V. The symmetry of the profiles with respect to $\omega = 0$ is lost. In the $TGB_A$ phase, the maximum is shifted from $\omega_L = 0$ towards $\omega_L > 0$. At 101.6 °C for instance, the shift is $\omega = 1.8$ degrees well beyond the uncertainty on the position of the peak ($\pm 0.3$ degrees). A more pronounced shift of $\omega_L$ towards positive values is measured close to the $TGB_A$–$TGB_C$ transition. On the other hand, the position of the peaks remains almost unchanged deep in the $TGB_C$ phase. All these observations indicate that the layer normal tilts over in response to a DC electric field to reach a new equilibrium value $\omega_L(T, V_{ext})$. The effect of a DC electric field is not limited to tilting the smectic layers: the two peaks of the $\omega$-scan recorded at 101.4 °C close to the $TGB_A$–$TGB_C$ transition (filled diamonds in Fig. 2b) have very different intensity. The peak corresponding to slabs with polarization parallel to the electric field ($\omega_L > 0$) is much more intense than its counterpart at $\omega_L < 0$ corresponding to slabs with polarization antiparallel to the electric field. This difference in intensity is a consequence of the other two phenomena discussed from equation (1):

(i) variation of the thickness $s_i$ of the smectic slabs and
(ii) $\chi$-reorientations [19,20].

The variations of the tilt angle (or else $TGB_C$ order parameter) $\omega_L(T, V_{ext})$ with temperature are plotted on Figure 3 for four different values of the applied voltage. The temperature scans go from the $TGB_C$ phase to the $TGB_A$. In the $TGB_C$ and for $V_{ext} = 0$, $\omega_L(T, 0)$ *vs.* temperature is represented by two symmetrical branches $\pm\omega_L$ corresponding to positions $(\omega_L, \chi = 0)$ and $(\omega_L, \chi = \pi)$ on the reciprocal rings. $\omega_L$ vanishes continuously upon heating at the $TGB_C$–$TGB_A$transition with a power law decay $t^\beta$ with $t = (T_{AC} - T)/T_{AC}$, $T_{AC} \approx 101.56$ °C and $\beta = 0.20 \pm 0.05$ [22]. When the DC electric field is applied, the behavior of the tilt angle $\omega_L$ depends strongly on the sign of the branch. The positive (negative) branch corresponds to scattering from slabs with polarization parallel (antiparallel) to $\mathbf{E}$ (*i.e.* $\chi = 0$ and $\chi = \pi$ respectively). Let us describe the behavior of the positive branch first. Deep in the $TGB_C$ phase, $\omega_L$ is not influenced by the field: the electroclinical effect is not detected far from the $TGB_C$–$TGB_A$transition, as expected. Upon approaching the $TGB_A$–$TGB_C$ transition, the tilt susceptibility becomes more important and the spontaneous $TGB_C$ tilt increases with the field. At the the transition temperature $T_{AC}$ and above in $TGB_A$ phase, a non zero tilt $\omega_L > 0$ is observed meaning that a layer tilt relative to the helical axis appears in response to the transverse DC electric field. Whatever the voltage, $\omega_L$ varies continuously at the $TGB_C$–$TGB_A$transition. Note that the positive branch looks very much like the behavior of an order parameter close to a second order transition in presence of a conjugated field (*e.g.* para to ferromagnetic transition under external magnetic field): the critical singularities at $t = 0$ disappear in the presence of the field. The negative branch exhibits a quite different behavior. $\omega_L(< 0)$ is again very close to the zero field value at low temperature in the $TGB_C$ phase, it shifts a little upon heating but disappears abruptly at some temperature $T^*$ below $T_{AC}$, the difference $(T_{AC} - T^*)$ increasing with the field. For $V_{ext} = 150$ V the negative branch even disappears for all measured temperatures in the $TGB_C$ range.

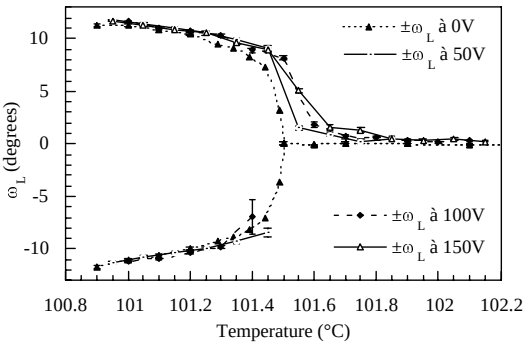


**Fig. 3.** Experimental results: $\omega_L$ *versus* $T$ by going from $TGB_C$ to $TGB_A$ for $V_{ext} = 0$ V, $V_{ext} = 50$ V, $V_{ext} = 100$ V and $V_{ext} = 150$ V. Estimated error bars on $\omega$ are drawn. Note that most of them are less than the symbol size.

We show now that the reported experiments can be qualitatively explained in terms of helically modulated electroclinical effect in a simple mean field phenomenological approach. The TGB free energy is constructed as

a Landau expansion in powers of the scalar (Ising) order parameter $\omega_L$. It reads, per unit area in the $y$-$z$ plane:

$$F_{AC} = \sum_{slabs\, i} \left\{ -EPs_i \sin\omega_{Li} \cos\chi_i + \frac{A}{2}\omega_{Li}^2 + \frac{B}{4}\omega_{Li}^4 + O(\omega_{Li}^6) + \frac{C}{2}(\omega_{Li+1} - \omega_{Li})^2 \right\} \quad (2)$$

$\omega_{Li}$ is the tilt angle of the smectic layers in slab number $i$ of thickness $s_i$ and orientation $\chi_i$ of the local polarization with respect to the external field. The first term in (2) is the electric contribution discussed in equation (1). The phase transition at zero field is controlled by the Landau expansion in even powers of $\omega_{Li}$ (symmetry $\omega_L \leftrightarrow -\omega_L$). It occurs for $A = 0$ at $T_{AC}$ and is second order in mean field for $B > 0$. In presence of the field, spatial modulations of $\omega_{Li}$ are expected. Their cost in energy is described by the gradient term $(C/2)(\omega_{Li+1} - \omega_{Li})^2$. At zero field, this term is minimum (and null) for a uniform value of $\omega_{Li}$. Since we focus on electroclinic effect, spatial modulations of slab thickness $s_i$ and orientation $\chi_i$ are neglected (see Ref. [20] for modelization of these effects) which amounts to postulate $\chi_i = i\,\Delta$ and $s_i = l_b$. Minimization of the free energy (2) for an infinite stack of discrete slabs is difficult. As usual, a continuous description is easier to handle and captures the same physics. Taking the continuous limit (*i.e.* infinite stack of slabs of infinitesimal thickness $s_i \to 0$ and orientation $\chi = 2\pi x/P$) we rewrite the free energy (2) per unit area in the $y$-$z$ plane and per pitch:

$$f = \frac{1}{2\pi}\int_0^{2\pi} \left\{ -\lambda\eta\cos\chi + \frac{r}{2}\eta^2 + \frac{u}{4}\eta^4 + \frac{\nu}{6}\eta^6 + \frac{c}{2}\left(\frac{d\eta}{d\chi}\right)^2 \right\} d\chi \quad (3)$$

$\eta = \sin(\omega_L(\chi, T, V_{ext})) \approx \omega_L$ denotes the new continuous order parameter of the $TGB_A$–$TGB_C$ transition. The new Landau coefficients $r$, $u$ and $c$ are proportional to $A$, $B$ and $C$ in (2). The gradient term is now a simple spatial derivative. The 6th order term has been added to the Landau expansion to include a possible tricritical behavior. At zero field, for $u > 0$, the $TGB_A$–$TGB_C$ transition is second order at $r = 0\,(T = T_{AC})$ and $\eta$ scales as $|T - T_{AC}|^{1/2}$. The transition is first order for $u < 0$ and tricritical for $u = 0$ with $\eta \propto |T - T_{AC}|^{1/4}$. The experimental order parameter exponent measured on our liquid crystal compound $\beta = 0.20 \pm 0.05$ [22] is marginally consistent with a tricritical mean field value; we shall therefore consider the tricritical condition $u = 0$, $\nu > 0$ in the following for numerical calculations. This restriction which may not apply to other $TGB_A$–$TGB_C$ systems is obviously of minor importance in the present model. Finally, the number of independent coefficients is reduced to two by an appropriate rescaling of the order parameter and of the energy:

$$F = \frac{2\pi f}{c}\left(\frac{c}{\nu}\right)^{-1/2} = \int_0^{2\pi} \left\{ -\Lambda\phi\cos\chi + \frac{R}{2}\phi^2 + \frac{1}{6}\phi^6 + \frac{1}{2}\left(\frac{d\phi}{d\chi}\right)^2 \right\} d\chi \quad (4)$$

in which the rescaled order parameter is $\Phi = \alpha\eta$ with $\alpha = (\nu/c)^{1/4}$. The parameters $\Lambda = \alpha\lambda/c$ and $R = r/c$ are proportional to the electric field amplitude $E$ and to the distance from the transition temperature $T$–$T_{CA}$. The stationary solution $\Phi(\chi)$ is obtained by solving the Euler-Lagrange equation of the free energy (4):

$$\frac{d^2\Phi}{d\chi^2} - R\Phi - \Phi^5 = -\Lambda\cos\chi. \quad (5)$$

Before we proceed to numerical resolution of (5), let us discuss the solutions $\Phi(\chi)$ in the limit of low electric field $|\Lambda/R| \ll 1$. For $R > 0$ ($TGB_A$), a particular solution of equation (5) reads:

$$\Phi_A(\chi) = \frac{\Lambda}{1+R}\cos\chi. \quad (6a)$$

The electric field induces a layer tilt $\Phi_A(\chi) \neq 0$ modulated by the TGB helical structure: $\Phi_A(\chi)$ is maximum for $\chi = 0$ and zero for $\chi = \pi/2$. In reciprocal space, the $TGB_A$ ring is rotated by a weak angle $\omega_L(T, V_{ext}) \approx \Phi_A(\chi)/\alpha$ about the $Q_y$ axis parallel to the field direction. An experimental $\omega$ scan at $\chi = 0$ [$\pi$] detects the shift of the maximum of scattering towards $\omega_L$ proportional to the field ($\Lambda \propto E$) and decreasing upon heating above $T_{CA}$. Note that a quadratic response (dielectric) would be proportional to $E^2 \propto \cos^2\chi$ and produce two maxima on an $\omega$ scan. In the $TGB_C$ phase in the low field limit ($|\Lambda/R| \ll 1$, $R < 0$), two solutions corresponding to the two Bragg rings $\Phi_{C+}(\chi)$ and $\Phi_{C-}(\chi)$ are found:

$$\Phi_{C\pm}(\chi) = \pm(-R)^{1/4} + \frac{\Lambda}{1-4R}\cos\chi. \quad (6b)$$

The two $TGB_C$ rings are rotated about the $Q_y$ axis in a symmetrical way preserving the inversion symmetry about the origin of reciprocal space. An $\omega$ scan at $\chi = 0$ would detect two peaks at positions $\omega_{L+} = \Phi_{C+}(0)/\alpha$ and $\omega_{L-} = \Phi_{C-}(0)/\alpha$ which are both shifted by the same amount, proportional to $E$ (with the same sign) and decreasing upon cooling far below $T_{CA}$.

In the general case, the non-linear differential equation (5) can be solved numerically. We used the D02RAF NAG Fortran routine. This routine solves the two-point boundary-value problem with general boundary conditions for a system of ordinary differential equations, using a deferred correction technique and Newton iteration. We impose periodic boundary conditions: $\Phi(0) = \Phi(2\pi)$ and $(d\Phi/d\chi)|_{\chi=0} = (d\Phi/d\chi)|_{\chi=2\pi}$. Figure 4 shows $\Phi_{C+}(0)$, $\Phi_{C-}(0)$ and $\Phi_A(0)$ *versus* $R$ for different values of $\Lambda$. $\Phi_{C-}(0)$ corresponds to smectic slabs with polarization anti-parallel to the electric field: the polarization decreases in response to the electric field and as consequence $\Phi_{C-}(0)$ and hence the tilt is lower than the equilibrium value in absence of the field. On the other hand, $\Phi_{C+}(0)$ refers to slabs with polarization parallel to the electric field and increases with the field. For weak values of the field $\Phi_{C+}(0)$ and $\Phi_{C-}(0)$ merge together at $R \approx 0$, then, for $R > 0$, only one stable solution $\Phi_A(0)$ exists corresponding

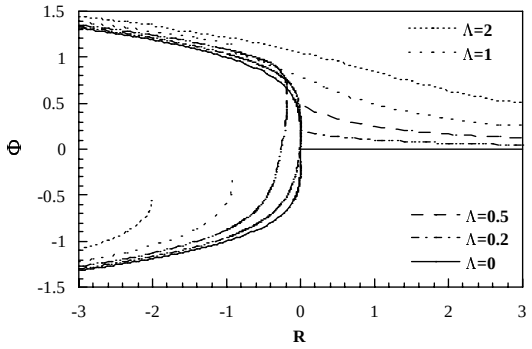


**Fig. 4.** Numerical results: order parameter $\Phi$ *versus* control parameter $R$ of the $TGB_C$–$TGB_A$ transition for $\Lambda = 0$, $\Lambda = 0.2$, $\Lambda = 0.5$, $\Lambda = 1$ and $\Lambda = 2$.

to a tilted $TGB_A$ phase. The evolution remains continuous: the single distorted ring splits up continuously into two rings. For higher values of the electric field ($\Lambda = 1$ and $\Lambda = 2$, in Fig. 4) a first order transition occurs at a critical temperature lower then $T_{AC}(R < 0)$, the numerical solution jumps from the field distorted two-branch solution $\Phi_{C\pm}(\chi)$ to the single branch $\Phi_A(\chi)$. The numerical solutions agree qualitatively well with the experimental results $\omega_L(\chi)$ *vs.* $T$ shown in Figure 3. In particular, the experimental discontinuous jump from two branches solution to one branch solution is well reproduced on the numerical curves. The change in intensity of the Bragg maxima upon increasing the field is however not described by the model since it corresponds to translations of grain boundaries as was discussed in reference [20].

In conclusion, the present paper demonstrates the existence of an electroclinical effect in TGB phases close to a $TGB_A$–$TGB_C$ transition. Although the phenomenological model is oversimplified, it supports the idea of a helical modulation of this effect and reproduces the main features of the observed behavior. A more accurate modelization should consider slabs of finite size, include translation of grain boundaries and rotation of smectic slabs.

## References

1. S. Garoff, R.B. Meyer, Phys. Rev. Lett. **38**, 848 (1977).
2. R. Qui, J.T. Ho, S.K. Hark, Phys. Rev. A **38**, 1653 (1988).
3. Ch. Bahr, G. Heppke, Phys. Rev. A **37**, 3179 (1988).
4. A.G. Rappaport, P.A. Williams, B.N. Thomas, N.A. Clark, M. Blanca Ros, D.M. Walba, Appl. Phys. Lett. **67**, 362 (1995).
5. J. Xue, N.A. Clark, Phys. Rev. Lett. **64**, 307 (1990).
6. S.-D. Lee, J. Patel, Phys. Rev. Lett. **65**, 56 (1990).
7. J.S. Patel, S.-D. Lee, J.W. Goodby, Phys. Rev. Lett. **66**, 1890 (1991).
8. W. Chen, Y. Ouchi, T. Moses, Y.R. Shen, K.H. Yang, Phys. Rev. Lett. **68**, 1547 (1992).
9. Z. Li, R.G. Petschek, C. Rosenblatt, Phys. Rev. Lett. **62**, 796 (1989); **62**, 1577(E) (1989).
10. Z. Li, G. Di Lisi, R.G. Petschek, C. Rosenblatt, Phys. Rev. A **41**, 1997 (1990).
11. S. Tripathi, M.H. Lu, E.M. Terentjev, R.G. Petschek, C. Rosenblatt, Phys. Rev. Lett. **67**, 3400 (1991).
12. K. Crandall, S. Tripathi, C. Rosenblatt, Phys. Rev. A **46**, R715 (1992).
13. J. Etxebarria, J. Zubia, Phys. Rev. A **44**, 6626 (1991).
14. R. Shao, J. Pang, N.A. Clark, J.A. Rego, D.M. Walba, Ferroelectrics **147**, 255 (1993); H.-S. Kitzerow, A.J. Slaney, J.W. Goodby, Ferroelectrics **179**, 61 (1996).
15. S.R. Renn, T.C. Lubensky, Phys. Rev. A **38**, 2132 (1988).
16. J.W. Goodby, M.A. Waugh, S.M. Stein, E. Chin, R. Pindak, J. Patel, Nature (London) **337**, 449 (1989); J. Am. Chem. Soc. **111**, 8119 (1989).
17. H.T. Nguyen, A. Boutcha, L. Navailles, P. Barois, N. Isaert, R.T. Twieg, A. Maaroufi, C. Destrade, J. Phys. II France **2**, 1889 (1992).
18. L. Navailles, R. Pindak, P. Barois, H.T. Nguyen, Phys. Rev. Lett. **74**, 5224 (1995).
19. M. Petit, P. Barois, H.T. Nguyen, Europhys. Lett. **36**, 185 (1996).
20. P. Barois, M. Nobili, M. Petit, Mol. Cryst. Liq. Cryst. **302**, 215 (1997).
21. L. Navailles, P. Barois, H.T. Nguyen, Phys. Rev. Lett. **71**, 545 (1993).
22. L. Navailles, Ph.D. thesis, Université Bordeaux 1, n° 1130, 1994.